# Model of Receiver Design Flaw – Crucial for Huygens Space Mission Recovery

L. Popken
European Space Agency
ESA/ESTEC, SCI-PS
Keplerlaan 1, PO Box 299
NL-2200 AG Noordwijk ZH, The Netherlands
Tel. +31-71-5654620
Luitjens.Popken@esa.int

*Abstract*—An analytical model is presented to recover from a current design flaw in the Huygens space mission relay-link receiver. The model of the faulty implementation of a Data Transition Tracking Loop (DTTL) is a driver for the trajectory redesign leading to the new relay-link geometry of the Huygens mission. This recovery shall allow for a successful data retrieval from the probe during its descent towards the Saturn moon Titan, despite the tracking deficiency in the given symbol synchronizer.
The model of the DTTL implementation is presented in terms of system-level parameters: Link Performance $(E_S/N_o)$, Symbol Transition Density $P_t$, and Input Symbol-Rate Offset $\Delta F$. The analytical model has undergone extensive successful verification during in-orbit tests and performance mappings since the discovery of the anomaly.

## TABLE OF CONTENTS



0-7803-8155-6/04/$17.00 © 2004 IEEE
IEEEAC paper # 1262, Vers. 3

## 1. BACKGROUND AND INTRODUCTION

The Cassini Spacecraft will reach Saturn in July 2004. It carries the Huygens Probe, which is scheduled for detachment from the orbiter towards the Saturn moon Titan in December 2004.

During the course of an in-orbit performance test in February 2000 a significant noncompliance of the probe relay receiver was detected. Subsequently, additional in-orbit performance mappings could only ascertain the receiver deficiency. Consequently, this would inflict substantial data losses if the originally foreseen probe mission with the corresponding relay-link geometry would have been proceeded as intended. Unfortunately, the earlier stage of the ground testing and verifications had failed to detect the problem, due to test coverage limitations.

To attempt for a re-design of the probe mission, it was crucial to identify what causes the technical anomaly, to provide an accurate and verified model for the given receiver characteristic and to predict reliably the remaining performances. The flaw was tracked down to be a design problem of the symbol synchronizer in the receiver, which is incompatible with the time-varying relative relay geometry of the originally foreseen mission profile and the (fixed) data rate (Doppler effect). This relay data rate is significantly higher than the usual uplink rates applied for spacecraft telecommanding, including the Cassini Orbiter.
[Note: Despite this unfortunate noncompliance with the original Huygens link geometry and the data rate, the implementation of the synchronizer suits very well for the lower telecommand data rates, usually applied in

common transponders and the actual design has, in fact, inherited such technical implementation.]

The Cassini/Huygens relay-link anomaly and recovery options have been presented by Dr. L. Deutsch at JPL in [6] from a system perspective. This paper focuses on the detailed and quantative modeling of the faulty synchronizer.

The symbol synchronizer implementation is based upon the well-established concept of the Data Transition Tracking Loop (DTTL). However, in the actual implementation the loop tracking performance is significantly degraded by a loop parameter setting, which is inadequate for the original mission. In addition, the performance is further constrained by two mutually dependent Automatic Gain Control (AGC) loops (noncoherent and coherent). The coherent AGC interacts directly with the DTTL such that the bandwidth and tracking capability of the synchronizer are discontinuous functions of the received signal power. Therefore, an increased receiver input power does not necessarily improve the tracking. On the contrary, it can cause loss of symbol synchronization in the given receiver. On the other hand, in no circumstance, the circuit can be reconfigured in-orbit by patching.

The paper illustrates a dynamical model for the symbol synchronizer, which is part of the receiver in the Probe Support Avionics (PSA) equipment onboard the Cassini Orbiter. The model describes the tracking performance of the synchronizer as function of system-level parameters: Link performance in terms of $E_S/N_o$; Symbol Transition Probability $P_t$; and input symbol rate Offset $\Delta F$, which depends upon the relative velocity from the relay-link geometry.

## 2. System and Signal Characteristics

The radio link between the Huygens Probe and the PSA onboard the Cassini Orbiter employs two RF channels for redundancy and uses a traditional modulation scheme. Sinusoidal subcarrier modulation is applied, and the symbol stream is phase-modulated onto a sinusoidal subcarrier at 131.072 kHz by applying binary-phase-shift-keying (BPSK). The nominal symbol rate is 16.384 ksymb/sec, which includes the channel coding redundancy in accordance with the CCSDS concatenated coding scheme of Reed Solomon (255,223) block coding and (R=1/2, k=7) convolutional coding [8].

The receiver performs the phase-coherent tracking of the residual-carrier in a second-order phase-locked loop (PLL). The phase-coherent demodulation of the subcarrier is achieved by a conventional second-order Costas-loop. Eventually, a traditional DTTL of first order accomplishes the symbol timing recovery and detection. The three loops for carrier-, subcarrier- and symbol-timing are closed after Analog-to-Digital Conversion (ADC) in the digital domain of the receiver.

The PSA equipment includes a Viterbi decoder circuit, but Reed Solomon (RS) decoding is not performed onboard. The received frames from the relay link, including the RS symbols, are inserted into the Cassini Orbiter telemetry after being stored temporarily onboard. The RS decoding is performed on ground at the Huygens operations center.

## 3. Synchronizer Architecture

The symbol synchronizer implementation follows the classical DTTL principle [7]. Fig. 1 shows a corresponding architectural block-diagram with the typical Mid-Phase and In-Phase symbol integration paths. Whenever there is a transition between adjacent symbols, the corresponding Mid-Phase integration provides an update for the estimated offset (or misalignment) of the actual time of sampling w.r.t. the center of the input symbol. This error signal is then used to adjust the frequency synthesizer which provides the sampling clock. For the Huygens application, a first-order DTTL is sufficient, i.e., there is no need for a loop filter ($F(s) = 1$), provided the loop gain is set adequately. If the update to the input of the synthesizer is provided less frequently, the phase excursions or timing misalignments are increasing, for a given frequency offset of the input symbol stream.

## 4. Analytical Model

The Huygens Probe mission has a wrong loop parameter setting in the symbol synchronizer implementation causing a loop bandwidth, which is too narrow. As a result, this significantly degrades the tracking capability of the first-order loop. On the other hand, because of the narrow bandwidth any jitter effect due to additive channel noise ($n(\cdot)$ in eq. 1) is negligible for the analysis of the timing-error process in the loop.

For the analytical model of the symbol synchronizer, the (absolute) timing-error $\epsilon(t)$ is represented by the normalized offset $\lambda = (\epsilon/T)$, where $T$ is the (binary) symbol duration on the channel. Given that the synchronizer is a digital implementation of the DTTL, it means that the evolution of the process $\lambda$ can be represented by a first-order non-linear difference equation

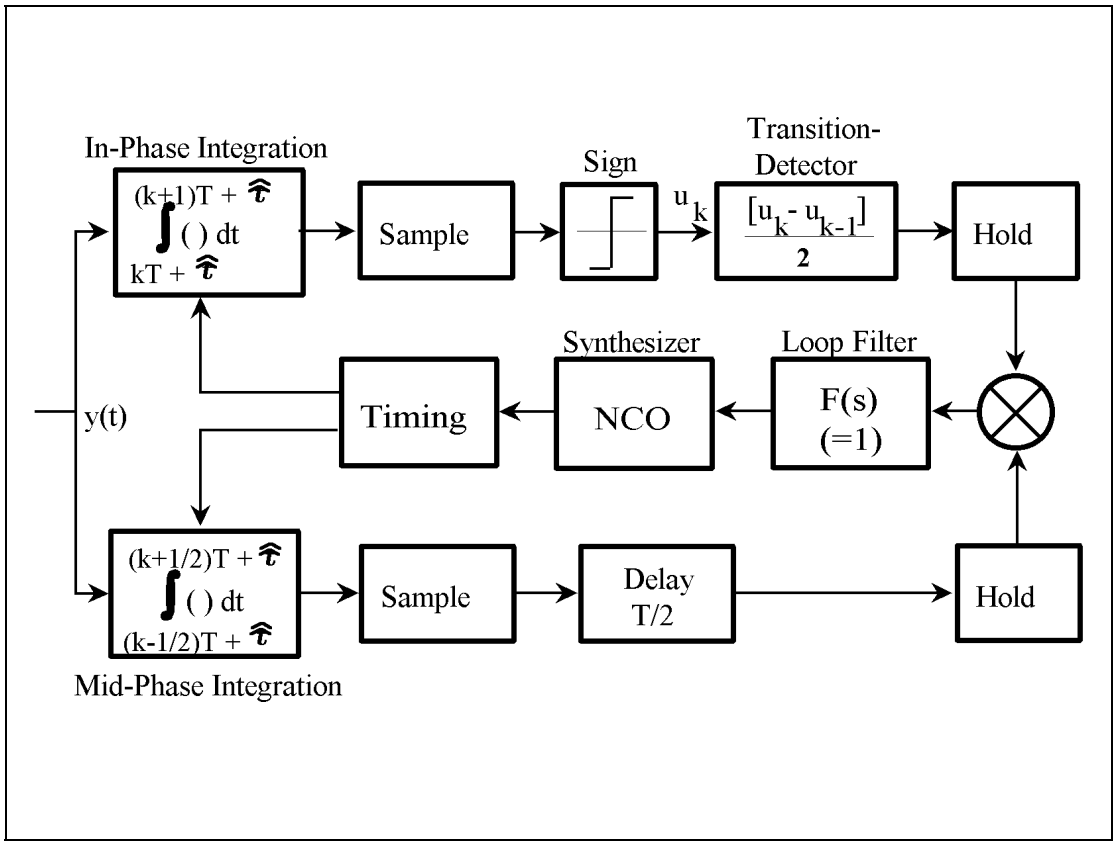


**Figure 1.** Principle of DTTL Symbol Synchronizer

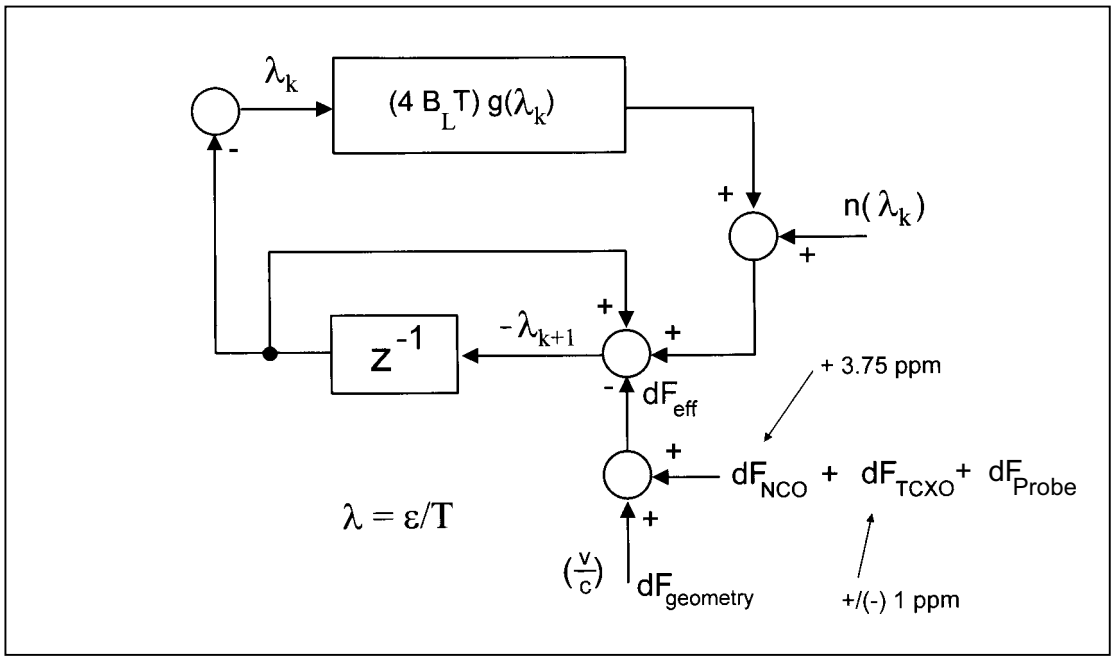


**Figure 2.** DTTL Dynamical Model

$$\lambda_{k+1} \;=\; \lambda_k - K\, g\left(\lambda_k, \frac{E_S}{N_o}, P_t\right) - n(\lambda_k) + \overbrace{\left(\frac{v}{c}\right) + dF_{Probe} + dF_{NCO} + dF_{TCXO}}^{F_{total}=dF_{eff}} \quad (1)$$

with (an arbitrary) $\lambda_{k=0}$=0, the relative velocity $v$ from the geometry, $c$ for the speed of light; $dF_{NCO}$ and $dF_{TCXO}$ are a known synchonizer NCO preset offset and the assumed receiver reference-clock worst-case offset (temperature-controlled crystal oscillator) respectively, with $F_{NCO}$=3.754 ppm, and $F_{TCXO}$=1.0 ppm. The factor $K$ is the open-loop gain, which is discussed in Sect. 5.

Fig. 2 is a block-diagram of the system equation in (1) with $K = (4B_LT)$, where $B_L$ is the one-sided noise bandwidth of the loop for a unit slope (or derivative w.r.t. $\lambda$) of $g(\cdot)$ at $\lambda$=0. The frequency tracking performance of the system is determined in terms of the offset

$$\triangle F = \left(\frac{v}{c}\right) + dF_{Probe} \quad (2)$$

at the DTTL input due to the Doppler effect $(v/c)$ and potential offsets $dF_{Probe}$ of the symbol clock generator in the transmitter onboard the probe. A relative velocity of 0.3 km/sec or 1080 km/h causes an input frequency offset of 1 ppm.

The function $g(\cdot)$ is the detector characteristic ($S$-curve). It represents the stochastic average of the *estimated* timing-offset ($\hat{\lambda}$) conditioned on the *actual* offset ($\lambda$). Its derivation requires statistical averaging of $\hat{\lambda}$ w.r.t. both noise and the random input symbol stream. The integrations in Fig. 1 are performed at symbol rate (16.384 ksymb/sec), while the effective loop bandwidth related to the dynamics of the process $\lambda$ is less than 1 Hz. For the selected time-discrete digital implementation of the DTTL, the integrate-and-dump filters process a large number (i.e., 248) of samples per each symbol. Therefore, the derivation of the detector characteristic $g(\cdot)$ may be based upon the assumption of a time-continuous loop operation. Although the derivation [2] of the $S$-curve requires statistical averaging, the difference equation for $\lambda_k$ in eq. (1) may be considered deterministic, i.e., the influence of the loop-noise $n(\lambda_k)$ on the tracking may be neglected in this special case. The function $g(\cdot)$ in eq. (1) is given by

$$g(\cdot) = (2P_t) \cdot \left[\lambda_k - \frac{1}{2}\left[1 + 2\lambda_k - P_t(1-2\lambda_k)\right] \cdot Q + \frac{1}{2}(1-P_t)(1-2\lambda_k) \cdot Q|_{\lambda_k=0}\right] \quad (3)$$

with

$$Q = \frac{1}{2} erfc\left((1-2\lambda_k)\sqrt{\frac{E_S}{N_o}}\right) \quad (4)$$

and $erfc(\cdot)$ for the Complementary Error-Function [9]. The $g(\cdot)$ in eq. (3) is valid for $0 \le \lambda \le 0.5$; it needs to be periodically extended w.r.t. $\lambda$ for the actual periodic $g(\lambda)$ according to

$$\begin{aligned} g(\lambda) &= -g(-\lambda) \\ g(\lambda \pm n) &= g(\lambda) \text{ for integer } n \end{aligned} \quad (5)$$

In [7] an $S$-curve $g(\cdot)$ for the DTTL is presented; however, the dependence on $P_t$ as a variable is not incorporated. The appendices summarize the derivation of $g(\cdot)$. Fig. 3 shows the non-linear $S$-curve with $E_S/N_o$ as parameter and for $P_t = 0.5$. The detector characteristic $g(\cdot)$ in eq. (3) can be normalized w.r.t. $(2P_t)$. Fig. 4 is a graph of the normalized detector characteristic for different values of $E_S/N_o$ and $P_t$ as parameters. The remaining dependency of the normalized $g(\cdot)/(2P_t)$ on $P_t$ is neglibible for $(E_S/N_o) > 8$ dB and, therefore, the corresponding curves overlap in Fig. 4.

## 5. Open-Loop Gain

Within the Analytical Model, the parameter $K$ in eq. (1) represents the critical open-loop gain, which determines the loop bandwidth of the DTTL. It is derived from the detailed implementation, which can be summarized as follows:

$$K = \sqrt{2}A \cdot \underbrace{G_{ADC}}_{ADC-Gain} \cdot \underbrace{K_{SL}}_{Short-Loop} \cdot \underbrace{[4 \cdot (F_{cl}T)]}_{Pre-Det./Decim.} \cdot \underbrace{K_{SW}}_{Scaling} \cdot \underbrace{\frac{1}{2}}_{Barrel} \cdot \underbrace{\left[\frac{(F_{cl}/8)}{2^{20}}\, T\right]}_{NCO} \quad (6)$$

where $\sqrt{2}A$ is the peak signal amplitude at the non-coherent AGC output; in Sect. 7 it is related to $E_S/N_o$. Further, it is $(1/T) = 16.384$ ksymb/sec for the nominal symbol-rate, and $F_{cl} = 4.0625$ MHz is the clock frequency, which drives the symbol synchronizer. The remaining parameters in eq. (6) are as follows:

*ADC-Gain*—The ADC has a width of 4 bits. Its wide-band input is dominated by noise, which is power-controlled by an analog non-coherent AGC to avoid excessive clipping effects at the ADC. The total ADC input power is 7 dBm, or 0.5 V rms across 50Ω. This implies an ADC Gain [10] of $G_{ADC}$=7.59 $V^{-1}$.

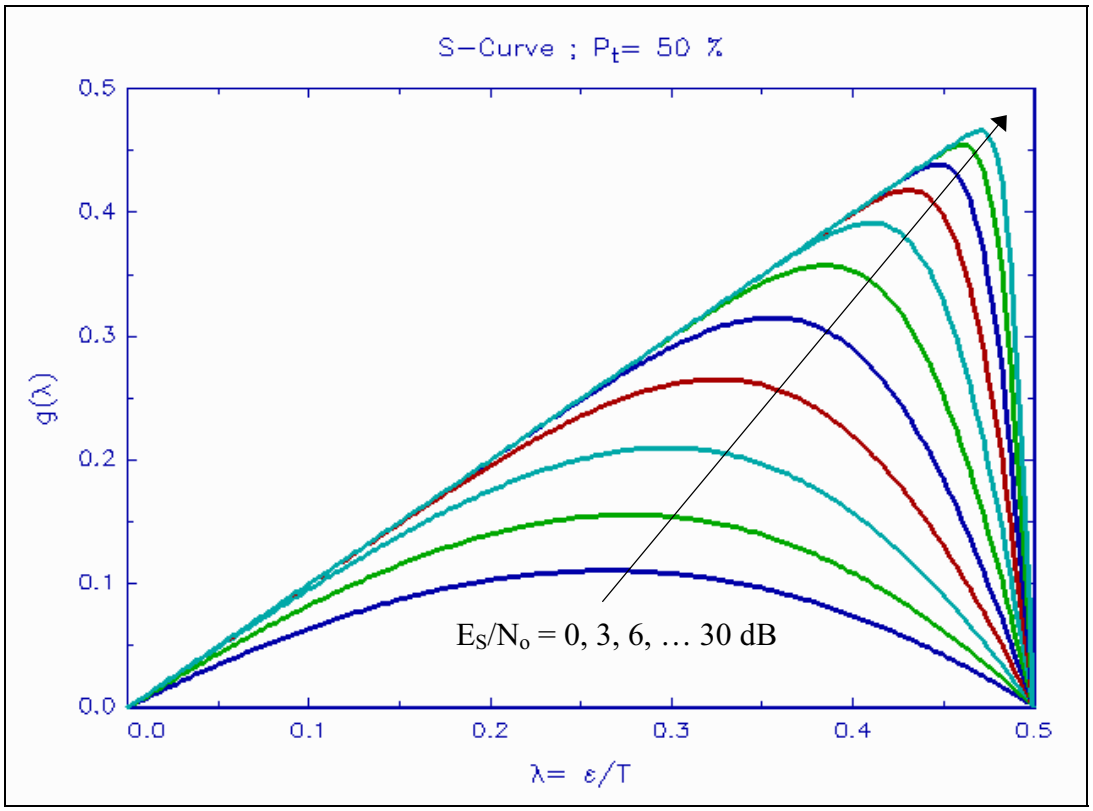


**Figure 3.** DTTL Detector Characteristic, with $E_S/N_o$ as Parameter

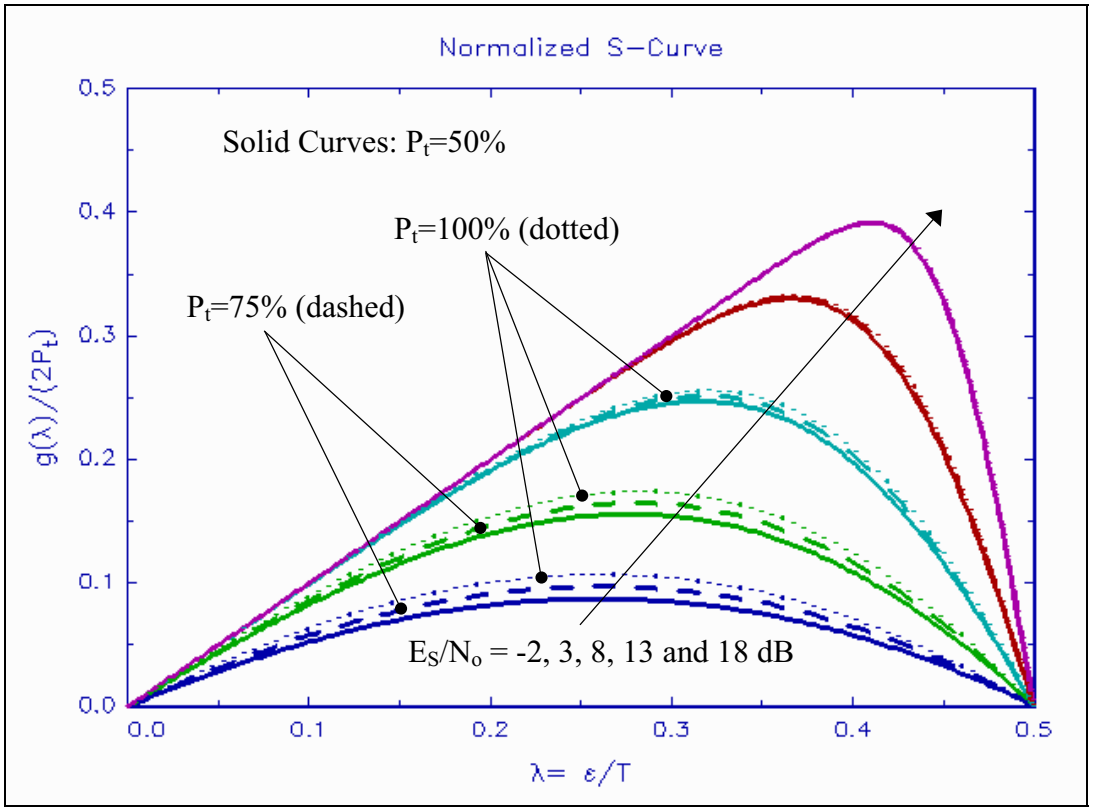


**Figure 4.** Normalized DTTL Detector Characteristic, with $E_S/N_o$ as Parameter

*Short-Loop Closure*— The receiver applies in the digital domain a short-loop closure with a corresponding conversion factor for the input signal amplitude. The parameter $K_{SL}$ in eq. (6) is proportional to the square-root of the ratio between data power $P$ and total signal power $A^2$. Therefore, $K_{SL}$ depends upon the modulation index $m$ with

$$K_{SL} \sim C_{SL} \cdot \sqrt{\frac{P}{A^2}} = C_{SL} \cdot \sqrt{2J_1^2(m)} \qquad (7)$$

with $C_{SL}$ for the amplitude conversion (gain/loss) factor of the short-loop downconversion and demodulation process, and $J_1(\cdot)$ for the first-kind Bessel-Function of first-order. The conversion factor can be obtained by simulation techniques or can be approximated by $C_{SL} \approx (2/\pi)\sqrt{2}$. Additionally, the parameter $K_{SL}$ will be used in Sect. 6 to calibrate the DTTL model for hardware implementation losses.

*Pre-Detection/Decimation*— The hardware implementation performs a pre-detection by summing four digital samples from the ADC. Instead of the time-continuous integrators as shown in Fig. 1, the digital DTTL circuit obtains the sum of a large number ($F_{cl}T = 248$) of samples of pre-detection outputs during each symbol period $T$.

*Scaling*—The output from the decimation or accumulation process is input to a microprocessor, which hosts the software for closing the loop operations of the DTTL (as well as the residual-carrier and subcarrier recoveries). For the timing recovery (first-order loop) the software performs a simple scaling by a factor of $K_{SW}$=$2^{-6}$. This particular selected scaling parameter is thus incompatible with the original Huygens mission link geometry and the relatively high symbol rate. An additional complication is subsisted by a digital coherent AGC function (Sect. 7), which can trigger a further reduction of the scaling factor towards $2^{-7}$ or even $2^{-8}$.

*Barrel-Shifter*—For the DTTL loop-closure, the microprocessor writes the scaled control signal to a register, which interfaces with the Numerically Controlled Oscillator (NCO). In order to accommodate both the results of the sign information from the In-Phase path and the Mid-Phase accumulation into the same register, the control signal is effectively divided by 2.

*NCO*— The NCO as part of the DTTL synthesizer in Fig. 1 is 20 bits wide and is clocked at $(F_{cl}/8)$. The corresponding term in eq. (6) represents the incremental minimum of cycles of the NCO output during the update period $T$ of the NCO and DTTL.

## 6. Model Calibration

During the development of the receiver the performance testing had revealed an implementation loss $L_{det}$ of 2.75 dB, and in special cases even 3 dB. Although significant, this loss (Non-Compliance Report NCR-385) was nevertheless accepted because of comfortable RF-Link margins for the original relay link geometry. The tests verified the system noise figure and required an increase of input signal power by 2.75 to 3 dB in order to achieve the theoretically expected bit-error rate (after convolutional decoding). The tests had applied frequency uncertainties w.r.t. the carrier, but unfortunately not w.r.t. the input symbol rate; otherwise the tracking deficiency of the symbol synchronizer would have been discovered. Therefore, in these tests the DTTL operated in the linear region and close to $\lambda \approx 0$, where the detector characteristic $g(\cdot)$ in Figs. 3 and 4 for relevant $E_S/N_o$ is almost independent of $E_S/N_o$.
After the detection of the anomaly, and when applying similar conditions, the in-orbit tests found [4] a consistent implementation loss $L_{im}$ of approximately 3.1 dB.

Part of this end-to-end loss $L_{det}$ is due to losses in the RF receive chain, in the short-loop closure, i.e,, the downconversion and demodulation behind the ADC, and eventually in the DTTL itself. This loss of approximately $L_{im}$ =1.8 dB is incorporated into the parameter $K_{SL}$ in eqs. (6) and (7) in order to calibrate the effective input signal amplitude and effectively the DTTL model for the hardware implementation loss,

$$K_{SL} = C_{SL} \cdot \sqrt{2J_1^2(m)} \cdot 10^{-L_{im}/20} \qquad (8)$$

The a-priori knowledge about the approximate loss was confirmed by the in-orbit test results reported in Sect. 10.

## 7. Automatic Gain Control

The probe relay-link receiver includes a wide-band non-coherent analog AGC, which maintains a constant 7 dBm total power of signal plus noise at the ADC input. In the digital domain of the receiver, a second narrow-band coherent AGC estimates the power of the residual-carrier. It applies an amplification or scaling such that at the input of the carrier-recovery a constant signal-level is available over the operational range of the receiver. This implies a nearly constant effective bandwidth of the carrier-recovery phase-locked loop. Fig. 5 shows the basic concept for the AGC functions in the receiver.

Considering a 50Ω system, in eq. (6) the peak signal

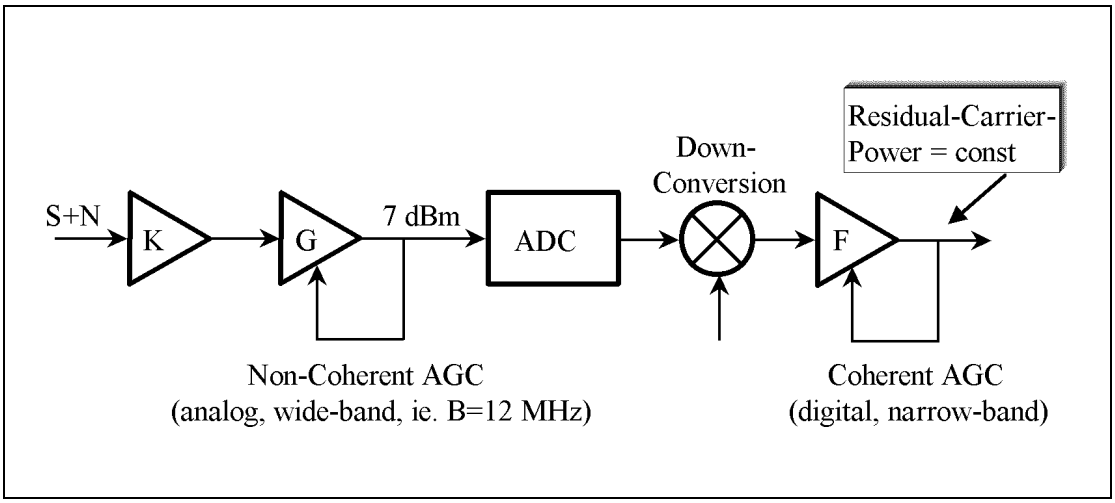


**Figure 5.** Principle of Automatic Gain Controls in Receiver

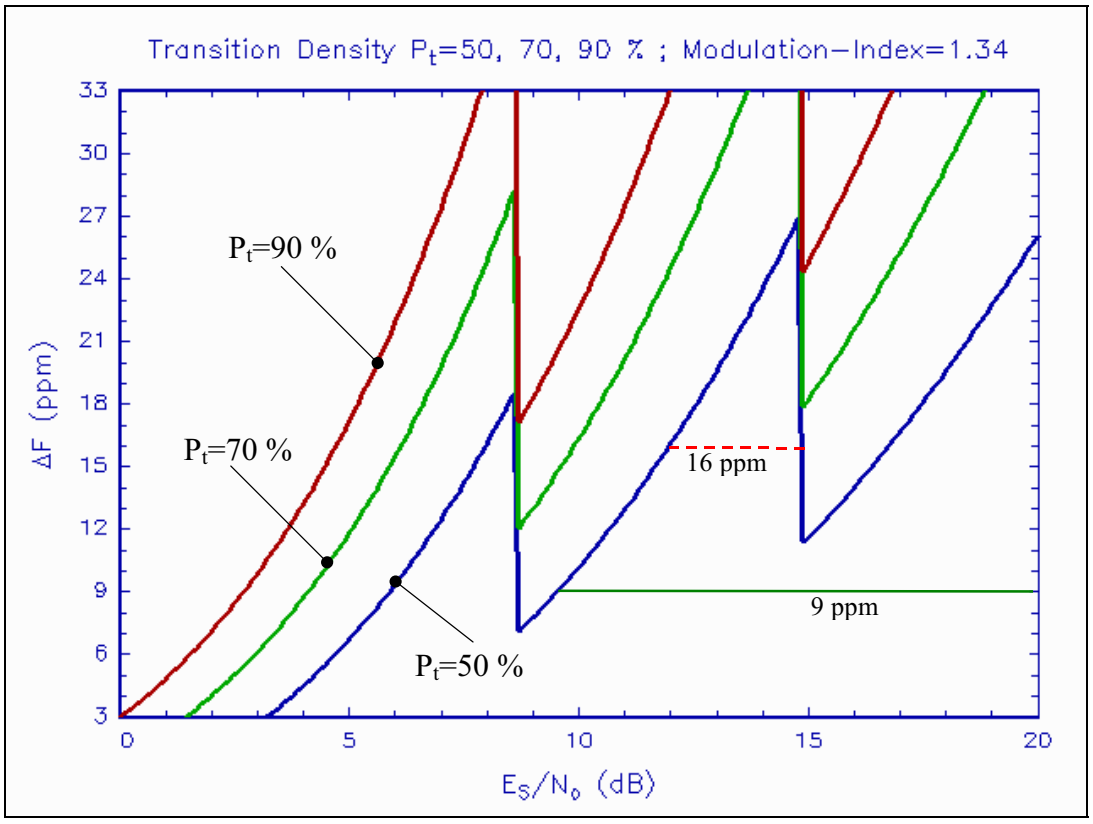


**Figure 6.** Model for Tracking Range of DTTL

amplitude $\sqrt{2}A$ (in $V$) at the output of the non-coherent AGC is given by

$$\sqrt{2}A = \frac{10^{P_{in}/20}}{\sqrt{10}\sqrt{1+SNR^{-1}}} \tag{9}$$

with $P_{in}$=7 dBm for the total power, and SNR for the (linear) signal-to-noise ratio, respectively, at the non-coherent AGC input. The SNR (in dB) is related to $E_S/N_o$ according to

$$SNR = (E_S/N_o) - 10\log(BT) - 10\log[2J_1^2(m)] \tag{10}$$

where $B = 12$ MHz is the nominal noise bandwidth at the non-coherent AGC input. This bandwidth may still be liable to vary for the in-flight equipment, since smaller bandwidths of 9.8 MHz and 11 MHz have been measured on engineering and qualification models of the receiver. Such diversity would imply a slight increase of SNR.

*Coherent AGC Switching-Points*

Further to the loop tracking performance, if the residual-carrier power at the input of the coherent AGC increases, the AGC will accordingly reduce its gain. When the AGC gain decreases below a specific preset value, the microprocessor which provides the NCO control word, will reduce the scaling factor $K_{SW}$ in eq. (6) by a factor of 2. If the residual-carrier power at the AGC input is increasing even further, the scaling $K_{SW}$ will eventually be affected by an additional division by 2.

The DTTL performances are evaluated in terms of the link parameter $E_S/N_o$ as an independent variable. However, the switching-points triggered by the coherent AGC depend upon the absolute power of the residual-carrier at the coherent AGC input, which for a given $E_S/N_o$ depends upon the modulation index $m$. Consequently, the switching-points if defined in terms of $(E_S/N_o)$-values, are changing with the modulation index, as for instance this index can vary with the probe temperature.

For the nominal modulation index $m$=1.34 rad, the two relevant switching-points of the DTTL dwell at $(E_S/N_o)$=8.64 dB and 14.84 dB respectively. Both switching-points were tested and verified during the in-orbit tests after corresponding link calibrations.

The modulation index $m$ may incur some uncertainties or variations. An increased (decreased) index requires an increase (decrease) in $E_S/N_o$ for a constant absolute residual-carrier power; this assumes a constant noise density $N_o$. Therefore, the switching-points are moving to higher (lower) values and, fortunately, into the same direction as the operating point $E_S/N_o$ is behaving. However, the absolute shifts are not identical [3].

Additionally, a change of input noise temperature as indicated by $N_o$, has some impact, while all other parameters are assumed constant. This change shall, for example, imply a reduction of $E_S/N_o$ from 8.6 dB (just below first switching-point) by 3 dB to 5.6 dB. The total power at the non-coherent AGC input is dominated by noise ((S/N)$< -5$dB). Therefore, the increase in $N_o$ by 3 dB implies a corresponding decrease by 3 dB in gain of the non-coherent AGC. Such gain adjustment will provide a decreased residual-carrier power to the input of the coherent AGC, which subsequently will apply a 3 dB higher gain. For the coherent AGC this represents an input operating point, which is 3 dB below the first switching-point.
By maintaining the increased noise temperature, it would need an increase of signal power, assuming constant modulation index, by the 3 dB in order to increase the $E_S/N_o$ towards the original 8.6 dB. As a result, the coherent AGC will operate again close to the first switching-point.

This example shows that the switching-points triggered by the coherent AGC are determined by specific values of the ratio $E_S/N_o$ and the modulation index $m$. Hence, the switching-points do not depend any further upon the absolute value of $E_S$ or $N_o$.

## 8. DTTL Tracking Performance

The characteristics of the DTTL can be subdivided into static tracking performance and the dynamics of cycle-slipping, in case the input offset exceeds the tracking range.

*Steady-State Tracking Limits*

Depending upon the system parameters of $(E_S/N_o)$, $P_t$, and $\triangle F$ in eq. (2), the process $\lambda_k$ in eq. (1) can reach a steady-state value

$$\lambda_{k+1} \rightarrow \lambda_k \rightarrow \text{const}\,.$$

In this case the DTTL is able to compensate for the input frequency offset, at the expense of a remaining static timing error, which degrades the symbol detection performance (Sect. 9). The corresponding maximum input frequency offset is given by

$$\Delta F_{max} = \left(\frac{v}{c}\right)_{max} + \, dF_{Probe} =$$

$$K \cdot g_{max}\left(\frac{E_S}{N_o}, P_t\right) - dF_{NCO} - dF_{TCXO} \quad (11)$$

where $g_{max}(\cdot)$ is the maximum of the $S$-curve in eq. (3) w.r.t. $\lambda$, for a given $E_S/N_o$ and $P_t$. The gain $K$ depends upon $E_S/N_o$ as per eq. (6) and Sect. 7 with the specific switching-points triggered by the coherent AGC. For three cases of Transition Densities $P_t = 50\%, 70\%,$ and $90\%$, the curves in Fig. 6 represent the tracking range in terms of maximum input frequency offset, with the discontinuities implied by the switching-points at $(E_S/N_o)$=8.64 dB and 14.84 dB. Similar curves were used to define several cases for the in-orbit tests and performance mappings of the DTTL. (Two specific offsets of 9 ppm and 16 ppm in Fig. 6 are addressed below.)

*Symbol Transition Density on Channel*

In Fig. 6 the tracking performance of the DTTL improves with increased Transition Density $P_t$. Random source data in the data-field of the transfer frame implies a $P_t$ close to 50 percent on the channel after the convolutional encoding. This density can be increased by inserting source packets, which include only "0" bits. Long sequences of 0's are converted by the convolutional encoding into alternating sequences of 0's and 1's with a "local" transition density of 100 percent. (The encoder performs symbol inversion on the output path of generator polynomial G2.) This increases the average $P_t$, and thus the DTTL performance. However, the insertion of such sequences requires an obvious reduction in effective telemetry capacity; therefore, it is not considered a suitable fix to the DTTL problem.

*Cycle-Slipping*

If the parameter-set of $(E_S/N_o)$, $\Delta F$ and $P_t$ in Fig. 6 implies an operating point above the corresponding "sawtooth" curve, the DTTL is unable to track the input frequency offset and will perform periodic cycle-slipping. Whenever the offset process $\lambda$ passes an odd-multiple of 0.5, i.e., (2j+1)0.5, a symbol will be lost or skipped in the detection process. For the Huygens Probe mission only positive frequency offsets are relevant, i.e., the incoming symbol stream is faster than nominal.

The model in eq. (1) allows to simulate the time interval, in terms of channel symbols, which the synchronizer needs to complete one cycle-slip. The Huygens telemetry frames are 16,384 symbols long. The DTTL dynamics in eq. (1) are slow relative to the symbol rate. Therefore, the time-discrete difference eq. (1) which represents the hardware implementation of the DTTL, may be approximated by a first-order differential equation for a time-continuous process $\lambda(t)$. This approach can be used to evaluate by integration the time $T_{cs}$ needed by the DTTL to complete one cycle-slip, i.e., the normalized process $\lambda(t)$ increases by 1. We obtain

$$T_{cs} = \frac{1}{16384} \cdot \left\{ \int_0^{0.5} \frac{d\lambda}{-K_{cal} \cdot g(\lambda, (E_S/N_o)) + F_{total}} + \int_{0.5}^{1} \frac{d\lambda}{K_{cal} \cdot g(1-\lambda, (E_S/N_o)) + F_{total}} \right\}$$

where $T_{cs}$ is given in terms of received transfer frames.

The malfunction of cycle-slipping is associated with loss of one symbol in the detection process per each cycle-slip. The symbol-loss, subsequently, upsets the channel decoding process [1] and the telemetry frame synchronisation of the PSA. The implied data loss in terms of affected transfer frames per cycle-slip can be related to the time interval $T_{cs}$, [1].

The well-established model also allows to simulate the tracking performance of the DTTL in a dynamic environment of time-varying parameters such as $E_S/N_o$ (for example, resulting from pendulum motion of the probe during its descent).

## 9. Symbol Detection Performance

The tracking and symbol synchronization by the DTTL are insufficient prerequisite for the successful detection of the information bits. In addition, the symbol error rate, which depends upon the tracking-error, must be less than approximately 10 percent. This allows the concatenated decoding scheme to achieve a rate of telemetry frame loss, which is low enough and acceptable for the radio link.

The effective $(E_S/N_o)_{eff}$ for the binary symbol detection can be estimated from

$$\left(\frac{E_S}{N_o}\right)_{eff} = \left(\frac{E_S}{N_o}\right) \cdot \frac{1}{L_{det}} \cdot (1 - 2|\lambda_k|)^2 \quad (12)$$

with $L_{det}$ for the detection implementation loss (worst case) introduced in Sect. 6, and $\lambda_k$ is the modulo-counted version of the process $\lambda_k$ in eq. (1), i.e., $|\lambda_k| \leq 0.5$ applies in eq. (12). For $P_t = 100\%$ the corresponding Symbol Error Rate (SER) is

$$SER = \frac{1}{2} erfc \sqrt{\left(\frac{E_S}{N_o}\right)_{eff}}. \quad (13)$$

The detection error rate depends upon the "local" or momentary transition density $P_{t,local}$ in the incoming symbol stream, and on the timing offset $\lambda$ by the DTTL. The process $\lambda$ is significantly slower than the symbol rate and depends on the *average* transition density $P_{t,average}$ over thousands of consecutive symbols, which assumes no cycle-slipping. If adjacent symbols are identical, the detection performance is not degraded by the timing-error at the sampling instant.

The momentary Symbol Error Rate is given by

$$SER = (1-P_{t,local})\frac{1}{2}erfc\sqrt{\left(\frac{E_S}{N_o}\right)\frac{1}{L_{det}}} + P_{t,local}\cdot$$

$$\frac{1}{2}erfc\left[\sqrt{\left(\frac{E_S}{N_o}\right)\frac{1}{L_{det}}}(1-2|\lambda(P_{t,average})|)\right] \quad (14)$$

for $|\lambda| \leq 0.5$. The first term considers identical adjacent symbols, and the corresponding detection error rate is negligibly small for the relevant $E_S/N_o$ on the link. The second term is much more significant and applies for different adjacent symbols.

Fig. 6 illustrates two example cases of frequency offsets, $\triangle F$=9 ppm (solid line) and $\triangle F$=16 ppm (dashed line). For these offsets Fig. 7 shows the corresponding SER as function of $E_S/N_o$ at the receiver input. The SER curves assume $P_t = 50\%$ and are constrained by the upper curve, which represents the error rate along the "sawtooth" tracking-limit in Fig. 6 for $P_t = 50\%$. The discontinuity in the SER performance for $\triangle F$=9 ppm is entailed by the switching-point in tracking performance in Fig. 6 at $(E_S/N_o)$=14.84 dB. Considering a fixed frequency offset, both the available tracking and detection margins in Figs. 6 and 7 increase while the operating point approaches a switching-point. On the other hand, when approaching a "sawtooth" from the right side the corresponding tracking margin becomes zero at the "sawtooth" curve, and the DTTL will start cycle-slipping.
An SER less than 10 percent requires a minimum $E_S/N_o$ of approximately 3 to 4 dB whenever the operating-point is close to a "sawtooth"-curve, [2].

## 10. Model Validation by Test

Fig. 8 is an example for the comparison between the Analytical Model as stated above and in-orbit test results. Below the limiting "sawtooth"-curve the symbol synchronizer does not show unlock phenomena ($\triangle$-points), and the data is successfully decoded. Above the limiting "sawtooth"-curve the system is unable to track the input offset $\Delta F$, ($\bigtriangledown$-points); intermediate performances are indicated by O-points. Overall, the outcome from the tests shows very good match of the model with the actual synchronizer performances. It should be noted that Fig. 8 does not represent any curve-fit of a model to measurement points, but instead it is a comparison between an a-priori established model and subsequent test results. Several independent in-orbit tests were used to validate the synchronizer model.

## 11. Recovery of Probe Relay-Link

The design of the new probe descent relative geometry must ensure the corresponding trajectory of input frequency offset $\Delta F$ and $E_S/N_o$ to fall in between or below the left and right "fingers" of the symbol synchronizer profile in order to minimize the risk of detection losses associated with entering a "finger".

Commonly, RF link budgeting is applied to guarantee under all mission conditions a *minimum* requirement for the signal strength, which is necessary for the RF link availability and the data retrieval. However, for the Huygens Probe mission the symbol synchronizer with its limitation imposes the additional constraint of a *maximum* allowed $E_S/N_o$ in order to avoid entering the right "finger". Essentially this upper limit and the need to optimize the time-varying link conditions for the available corridor between the "fingers" require an RF link modeling approach different from the usual budgeting and corresponding margin policies.

An example for the revised mission profile is illustrated in Fig. 9 and has been applied during the in-orbit tests. Each arrow-marker represents the average of $E_S/N_o$ within 10 minutes time interval during the probe descent. For each time interval, the left and right crosses indicate the absolute minimum and maximum values of $E_S/N_o$, respectively.

The relay-link modeling [3] is based upon two elements:

- A static Reference Link Budget (RLB) establishes a reference-point for $E_S/N_o$. This budget includes the usual electrical link parameters. However, the following entries: (1) relative distance between Huygens Probe and Cassini Orbiter, (2) probe antenna gain, (3) polarization mismatch between probe antenna and Cassini High-Gain Antenna (HGA), and (4) HGA pointing-offset depend upon the relative geometry, and thus are time-varying. For these parameters the RLB considers some reference values but no corresponding variations or uncertainties. Tab. 1 shows an RLB summary for one of the two RF channels and for the nomi-

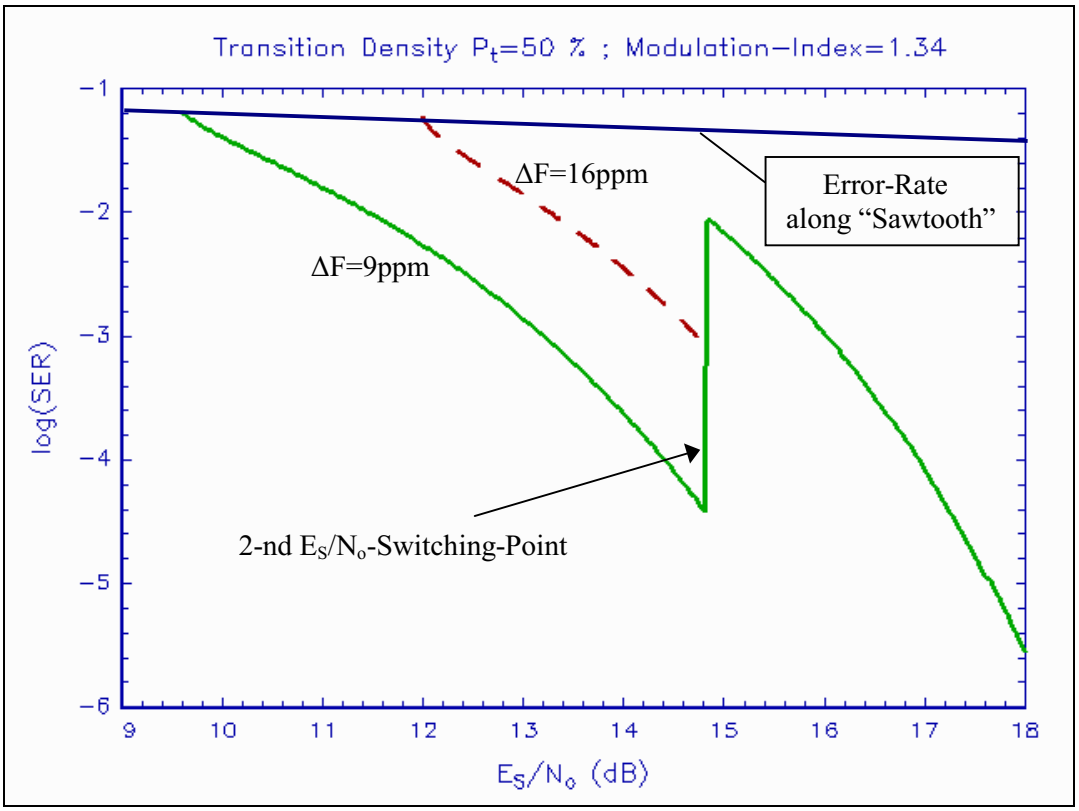


**Figure 7.** Symbol Error Rate affected by DTTL Tracking Performance

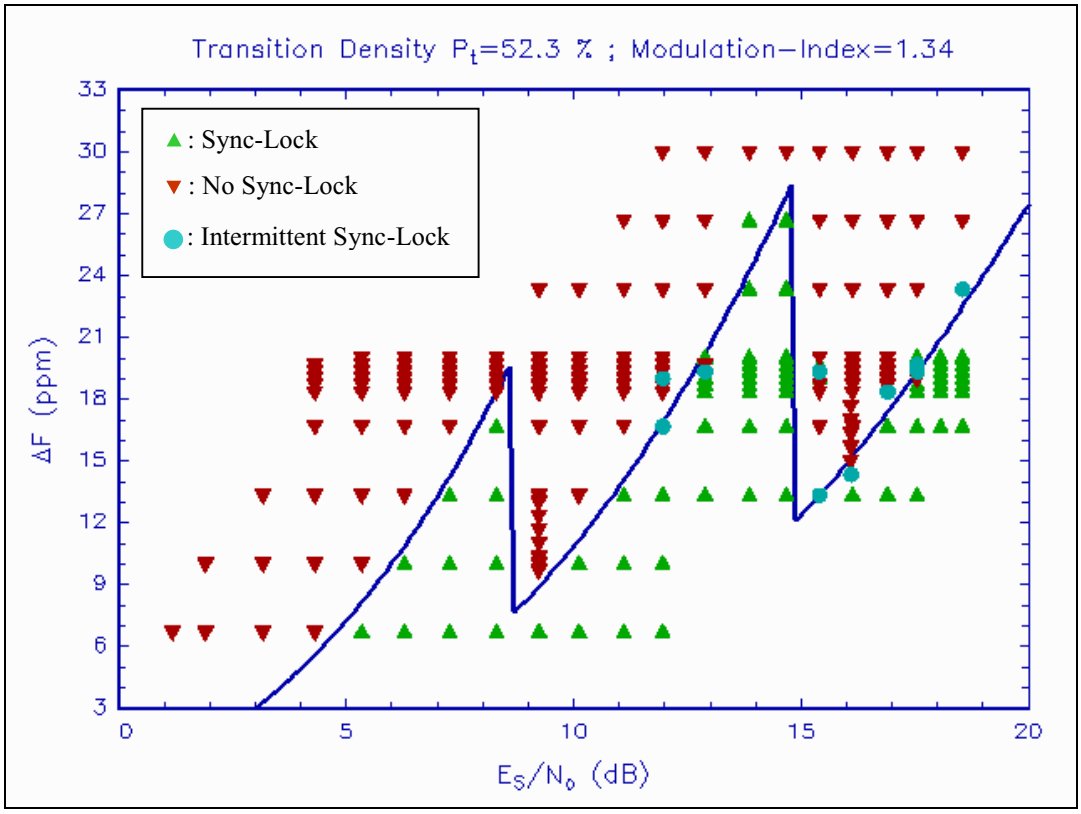


**Figure 8.** Comparison of Synchronizer Model and In-Orbit Test Results

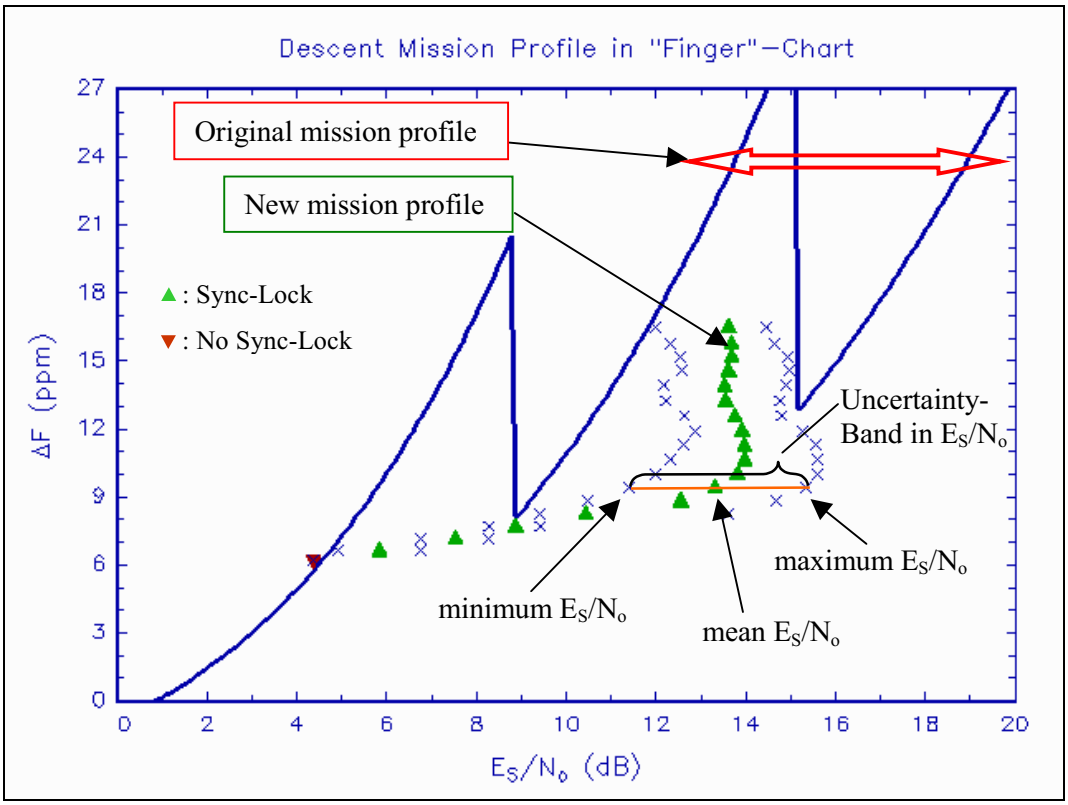


**Figure 9.** Example of the new Relay-Link Profile vs. Symbol Synchronizer Performance

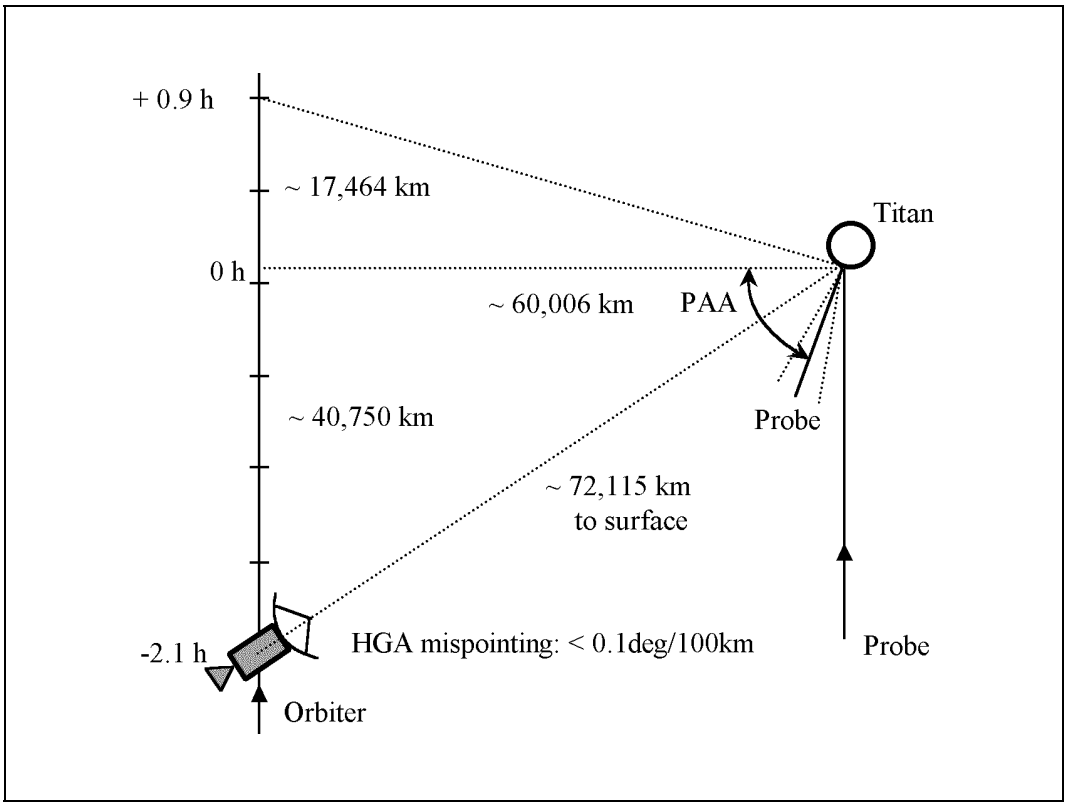


**Figure 10.** Revised Relay-Link Geometry [5]

nal *reference* $E_S/N_o$.

• A Descent Trajectory Analysis Tool (DTAT) models the variation and uncertainties of the geometry dependent entries, for which the RLB considers (only) reference values. Accordingly, the DTAT adjusts the reference $E_S/N_o$ from the RLB to the actual $E_S/N_o$ during the probe descent. It also models the corresponding band of variation or uncertainty of $E_S/N_o$.

The reference $E_S/N_o$ from the RLB is associated with an overall uncertainty due to electrical performance variations, which are independent of the link geometry. The total uncertainty of the predicted $E_S/N_o$ is determined in the DTAT by combining the constant uncertainty from the RLB with the variations, which are geometry dependent. The detailed link-budget modeling is given in [3].

**Table 1**. Summary of Probe Relay RLB.

| Parameter | Value | Comment |
|---|---|---|
| Probe RF Power | 10.66 dBW | nominal |
| Mismatch Loss | 0.20 dB | VSWR<1.5 |
| Circuit Losses | 0.22 dB | |
| Probe ANT Gain | 3.46 dBi | DTAT-modeled |
| Probe EIRP | 13.70 dBW | |
| | | |
| Frequency | 2.04 GHz | |
| Distance | 60000 km | DTAT-modeled |
| Space Loss | 194.2 dB | |
| Atmospheric Loss | 0.05 dB | |
| Tx Pol Ax-Ratio | 1.62 dB | DTAT-modeled |
| Rx Pol Ax-Ratio | 4.2 dB | max in HPBW |
| Polarization Loss | 0.19 dB | DTAT-modeled |
| Propagation Loss | 194.45 dB | total |
| | | |
| Rx Ant Gain, pk. | 35.05 dBi | Cassini HGA |
| HGA Point. Loss | 0.0 dB | DTAT-modeled |
| | | |
| Input Noise | 90 K | Titan, nominal |
| Noise Figure | 2.57 dB | System [3] |
| G/T | 10.9 dB/K | |
| Rx Power | -116.15 dBm | Rx-Syst. Input |
| | | |
| Modulation Index | 1.34 rad | nominal |
| Data Mod.-Loss | 2.50 dB | nominal |
| Symbol-Rate | 42.14 dBHz | 16.384 ksymb/s |
| | | |
| **$E_S/N_o$** | **14.11 dB** | Reference |

*Revised Relay-Link Geometry*

In order to avoid data losses originated by cycle-slipping in the symbol synchronizer, the original link geometry has been modified radically [1], [5]. For the new relay geometry the Cassini Orbiter and Huygens Probe will fly side-by-side at a large distance (Fig. 10). At the periapsis the Doppler effect is zero. Ideally, one should have an Orbiter Delay Time (ODT) of 1.5 hrs such that the 3 hours of probe relay link are symmetrically around periapsis and the Doppler effect is minimum. However, due to Probe Aspect Angle (PAA) constraints, the ODT could not be reduced to less than 2.1 hrs. The PAA represents an important parameter for the link, because it determines the effective probe antenna gain.

## 12. Lessons Learned

The Huygens relay-link design flaw incident provides valuable lessons to be learned and worthwhile to be retained [1], [6]. This paper highlights the following observations related to the DTTL design problem.

The relay-link receiver is inherited from standard S-Band transponders with telecommand rates not exceeding 2 kbit/sec. The symbol rate of 16 ksymb/sec for the Huygens application is significantly too high. During the development phase, the difference between 2 and 16 ksymb/sec rates did not trigger any detailed revalidation or specific testing of the current DTTL design for the high symbol rate.
Although a design may be inherited from previous missions, the existing performance values should not be taken for granted but instead re-evaluated with the requirements of the new application and possible adaptations to be identified for the design. Rigorous design revalidation and testing in all relevant aspects is mandatory. The Huygens relay-link receiver development, obviously, diverted from such approach.

The original transponder design from which the receiver had been derived, included a significant degree of in-orbit reconfigurability by telecommand. This included switchable data rates and the feature to adjust the bandwidth settings for carrier and subcarrier loops as well as for the DTTL symbol synchronizer. In fact, the Huygens original probe mission did not require any such reconfigurability. Therefore, such flexibility was probably considered as an unnecessary design complexity or avoidable risk. The original reconfigurability had thus been completely eliminated from the original design by hardware settings. The in-orbit receiver lacks the flexibility for modification by command or to

have its basic synchronization and loop parameters being patched.
Some in-orbit reconfigurability at unit level is good practice for an engineering approach. This allows to cope with unforeseen circumstances, such as in-orbit failures or the discovery of design deficiencies as in the case of the Huygens receiver. The advantage of such flexiblity is by far more important than a corresponding increase, if any, in design complexity. System parameters can, for instance, be stored in EEPROM or Flash-Memory and copied to registers of the hardware implementation during bootup. Beyond the modification of system parameters, in the future the architecture of the in-orbit (synchronization) system itself may also be reconfigurable by using RAM-based Field-Programmable Gate-Arrays, as an example. The configuration data is stored in EEPROM or Flash, which can be patched by telecommand.
[Note: **IF** the original reconfigurability were still available in the receiver, it would have been very easy to fix the DTTL problem.]

When assessing the RF link-budget for the "original mission profile" in Fig. 9, the margin of the available symbol $E_S/N_o$ is by far large. The link requires neither concatenated nor any convolutional channel coding [8] for the retrieval of the data.
It is interesting to observe that during the system development phase the onboard complexities (implied by concatenated channel coding with onboard convolutional decoding and frame synchronization) were considered acceptable, although these are not required by the mission. On the other hand, the switchable receiver loop bandwidths were eliminated from the original design. In retrospect, this inconsistency can be seen as an imbalance in the design integrity and its risk management.
By far and large, if the unnecessary concatenated channel coding - or at least the convolutional part (r=1/2) - would be a switchable option on probe transmitter and relay receiver, the symbol rate could be reduced by at least 50 percent. The existing DTTL would be able to track the lower symbol rate without difficulty, and no re-design of the relay link geometry would have been necessary for the mission recovery.

## 13. Conclusion

The symbol synchronizer in the relay-link receiver of the Huygens Probe mission is significantly incompatible with the given data rate and the originally baselined time-varying link geometry. Extensive efforts for a verified Analytical Model of the flaw were spent to cater at system level for the deficiency of the receiver. Successful verification and in-orbit testing were pursued following the flaw's detection. In addition, with accurate predictable link-budget performance, the model defines the remaining operational corridor of the receiver.

The Analytical Model was a major step forward and represents the core input to the redesign of the Huygens Probe and for the new orbiter/probe relative geometry. Eventually, this recovery is a prerequisite for the successful data retrieval from the Huygens Probe during its unique mission to the Saturn moon Titan.

## 14. Acknowledgements

Appreciation goes to Dr. Lorenzo Simone for providing the implementation parameters of the hardware presented in Sect. 5. Special thanks go also to Ferial Chummun for her editorial revision of the paper.

## 15. Appendices

The series of Appendices hereafter outlines the derivation of the DTTL $S$-curve as function of $E_S/N_o$ and $P_t$.

*Appendix A*

The DTTL input $y(t) = s(t,\tau)+n(t)$ in Fig. 1 consists of the signal

$$s(t,\tau) = \sqrt{P} \sum_{j=-\infty}^{\infty} a_j p(t - jT - \tau)$$

and $n(t)$ for additive white Gaussian noise (AWGN) of one-sided spectral density $N_o$ in W/Hz. The pulse $p(t)$ may be considered rectangular with unit amplitude. The binary ($\pm 1$) symbol stream $a_j$ is random with Transition Density $P_t$. Other parameters are $P$ for the symbol signal power, $T$ for the symbol duration, and $\tau$ representing an arbitrary delay of the input signal, to which the DTTL needs to be synchronized.

The sampled output of the In-Phase integration (Fig. 1) is given by

$$y_{I,k} = \int_{kT+\hat{\tau}}^{(k+1)T+\hat{\tau}} s(t,\tau)dt + \int_{kT+\hat{\tau}}^{(k+1)T+\hat{\tau}} n(t)dt$$

or

$$y_{I,k} \hat{=} b_k + n_{1,k}$$

with $n_{1,k}$ for a zero-mean Gaussian random variable of variance $N_o(T/2)$, and the random In-Phase signal component

$$b_k = \sqrt{P}\,[a_{k+1}(1-\lambda)T + a_{k+2}\lambda T] \qquad \text{(A.1)}$$

where we introduce the delay parameter $\lambda$ with

$$0 \leq \lambda = \frac{\tau - \hat{\tau}}{T} \leq \frac{1}{2} \,. \qquad \text{(A.2)}$$

To simplify notations we assume positive delays; the outcome in eq. (A.1) can obviously be modified for negative $\lambda$ by considering $a_k$ instead of $a_{k+2}$, and replacing $\lambda$ by $|\lambda|$. A positive delay represents a too far late sampling of the In-Phase integration. Therefore, the integration result over $T$ in eq. (A.1) comprises only a fractional weighting $(1-\lambda)$ of the (nominal) symbol $a_{k+1}$, and additionally a weighting $(\lambda)$ of the next following symbol $a_{k+2}$.

Similarly, we obtain for the sampled Mid-Phase integration (Fig. 1)

$$y_{M,k} = \int_{(k-1/2)T+\hat{\tau}}^{(k+1/2)T+\hat{\tau}} s(t,\tau)dt + \int_{(k-1/2)T+\hat{\tau}}^{(k+1/2)T+\hat{\tau}} n(t)dt$$

or

$$y_{M,k} \hat{=} c_k + n_{2,k}$$

with $n_{2,k}$ for a zero-mean Gaussian random variable of variance $N_o(T/2)$, and the random Mid-Phase signal component

$$c_k = \sqrt{P}\left[a_k(\frac{1}{2}-\lambda)T + a_{k+1}(\frac{1}{2}+\lambda)T\right] \,. \qquad \text{(A.3)}$$

The noise terms $n_{1,k}$ and $n_{2,k}$ are correlated due to their partial time-overlap of $(T/2)$, which enables each term to be represented by two components

$$n_{1,k} = u_{1,k} + v_{1,k}$$

$$n_{2,k'} = u_{2,k'} + v_{2,k'}$$

with

$$u_{1,k} = \int_{kT+\hat{\tau}}^{(k+1/2)T+\hat{\tau}} n(t)\,dt$$

$$v_{1,k} = \int_{(k+1/2)T+\hat{\tau}}^{(k+1)T+\hat{\tau}} n(t)\,dt$$

and

$$u_{2,k'} = \int_{(k'-1/2)T+\hat{\tau}}^{k'T+\hat{\tau}} n(t)\,dt$$

$$v_{2,k'} = \int_{k'T+\hat{\tau}}^{(k'+1/2)T+\hat{\tau}} n(t)\,dt$$

All four terms $u_{1,k}, v_{1,k}, u_{2,k'}$ and $v_{2,k'}$ are zero-mean Gaussian random variables with variance

$$\sigma^2 = N_o(T/4) \,. \qquad \text{(A.4)}$$

The terms are mutually independent, with the exception of

$$\begin{aligned} u_{1,k} &= v_{2,k'} \text{ for } k' = k \,, \\ v_{1,k} &= u_{2,k'} \text{ for } k' = (k+1) \,. \end{aligned}$$

In the In-Phase integration path of the DTTL (Fig. 1) the signs of two subsequent integrator outputs are processed to detect any symbol transition and its direction. The Mid-Phase integration result is delayed by half a symbol and then multiplied with the transition detector output to obtain the loop error signal

$$\begin{aligned} e_k &= (c_k + u_{2,k} + v_{2,k}) \cdot \\ &\quad \frac{1}{2}\left[sgn\left(b_k + u_{1,k} + v_{1,k}\right) - \right. \\ &\quad \left. sgn\left(b_{k-1} + u_{1,(k-1)} + v_{1,(k-1)}\right)\right] \end{aligned}$$

Next, a conditional averaging is performed on $e_k$ w.r.t. the additive noise, considering a given symbol sequence in terms of $b_{k-1}, b_k$ and $c_k$.

$$\begin{aligned} \mathbf{E}(e_k) = \frac{1}{2}( & c_k \mathbf{E}(sgn\left(b_k + u_{1,k} + v_{1,k}\right)) \\ & - c_k \mathbf{E}(sgn\left(b_{k-1} + u_{1,(k-1)} + v_{1,(k-1)}\right)) \\ & - \underbrace{\mathbf{E}(u_{2,k} \cdot sgn\left(b_{k-1} + u_{1,(k-1)} + v_{1,(k-1)}\right))}_{E_1} \\ & - \underbrace{\mathbf{E}(v_{2,k} \cdot sgn\left(b_{k-1} + u_{1,(k-1)} + v_{1,(k-1)}\right))}_{0} \\ & + \underbrace{\mathbf{E}(v_{2,k} \cdot sgn\left(b_k + u_{1,k} + v_{1,k}\right))}_{E_2} \\ & + \underbrace{\mathbf{E}(u_{2,k} \cdot sgn\left(b_k + u_{1,k} + v_{1,k}\right))}_{0} \,) \end{aligned}$$

For a given $b_j$ it is easy to derive (Appendix B)

$$\mathbf{E}(sgn\left(b_j + u_{1,j} + v_{1,j}\right)) = erf\left(\frac{b_j}{2\sigma}\right)$$

with $erf(\cdot)$ for the Error-Function [9]. In order to evaluate the above average $E_1$ we notice that $u_{2,k} \equiv v_{1,(k-1)}$, which is statistically independent of $u_{1,(k-1)}$. It is then straightforward to obtain (Appendix C)

$$E_1 = \frac{\sigma}{\sqrt{\pi}} \exp\left(-\frac{3\,b_{k-1}^2}{4\sigma^2}\right)$$

and a corresponding result for $E_2$ by inserting $b_k$ instead of $b_{k-1}$. The average of the loop error signal can then be reformulated as

$$\mathbf{E}(e_k) = \frac{1}{2}\left[c_k \cdot erf\left(\frac{b_k}{2\sigma}\right) - c_k \cdot erf\left(\frac{b_{k-1}}{2\sigma}\right)\right.$$

$$-\frac{\sigma}{\sqrt{\pi}}\exp\left(-\frac{3\,b_{k-1}^2}{4\sigma^2}\right)+\frac{\sigma}{\sqrt{\pi}}\exp\left(-\frac{3\,b_k^2}{4\sigma^2}\right)\Bigg] \tag{A.5}$$

This average is conditioned on $b_{k-1}$, $b_k$ and $c_k$, which per eqs. (A.1) and (A.3) depend upon the random input symbol stream $a_k$, $a_{k+1}$ and $a_{k+2}$, and the delay $\lambda$.

It remains to average the mean value in eq. (A.5) w.r.t. all possible sequences of the input symbol stream with the corresponding probabilities of occurence. For this purpose Tab. A.1 shows the eight possible cases of sequences for three consecutive input symbols and their probabilities in terms of $P_t$. Tab. A.2 provides the corresponding values of $b_{k-1}$, $b_k$ and $c_k$ as needed in eq. (A.5).

**Table A.1**. Sequence of three Symbols and corresponding Probabilities.

| Case | Probability | $a_k$ | $a_{k+1}$ | $a_{k+2}$ |
|---|---|---|---|---|
| 1 | $\frac{1}{2}(1-P_t)^2$ | -1 | -1 | -1 |
| 2 | $\frac{1}{2}(1-P_t)P_t$ | -1 | -1 | 1 |
| 3 | $\frac{1}{2}P_t^2$ | -1 | 1 | -1 |
| 4 | $\frac{1}{2}P_t(1-P_t)$ | -1 | 1 | 1 |
| 5 | $\frac{1}{2}P_t(1-P_t)$ | 1 | -1 | -1 |
| 6 | $\frac{1}{2}P_t^2$ | 1 | -1 | 1 |
| 7 | $\frac{1}{2}(1-P_t)P_t$ | 1 | 1 | -1 |
| 8 | $\frac{1}{2}(1-P_t)^2$ | 1 | 1 | 1 |

**Table A.2**. In-Phase and Mid-Phase Signal Components, corresponding to Table A.1.

| Case | $b_{k-1}/\sqrt{P}$ | $b_k/\sqrt{P}$ | $c_k/\sqrt{P}$ |
|---|---|---|---|
| 1 | $-T$ | $-T$ | $-T$ |
| 2 | $-T$ | $2\lambda T-T$ | $-T$ |
| 3 | $2\lambda T-T$ | $-2\lambda T+T$ | $2\lambda T$ |
| 4 | $2\lambda T-T$ | $T$ | $2\lambda T$ |
| 5 | $-2\lambda T+T$ | $-T$ | $-2\lambda T$ |
| 6 | $-2\lambda T+T$ | $2\lambda T-T$ | $-2\lambda T$ |
| 7 | $T$ | $-2\lambda T+T$ | $T$ |
| 8 | $T$ | $T$ | $T$ |

For each Case the signal components as per Tab. A.2 are inserted into eq. (A.5) and the resulting mean value is weighted by the corresponding probability in Tab. A.1. This leads to 8x4=32 terms contributing to $\mathbf{E}(e_k)$, which can be simplified by combining terms straightforward leading to the following result

$$\frac{\mathbf{E}(e_k)}{\sqrt{P}T}=g(\cdot)=(2P_t)\cdot\frac{1}{4}\Bigg[[1+2\lambda -P_t(1-2\lambda)]\,erf\left((1-2\lambda)\sqrt{\frac{E_s}{N_o}}\right) +(1-P_t)(2\lambda-1)\,erf\left(\sqrt{\frac{E_s}{N_o}}\right)\Bigg] \tag{A.6}$$

where we used

$$\frac{\sqrt{P}T}{2\sigma}=\sqrt{\frac{E_S}{N_o}} \tag{A.7}$$

with $(E_S/N_o)$ for the symbol-energy-to-noise-density ratio at the DTTL input.

Combining the various (32) contributing terms can be much simplified by making use of symmetries of the elements in Tabs. A1 and A2. Applying the Complementary Error-Function $erfc(\cdot)=1-erf(\cdot)$ leads to the detector charateristic $g(\cdot)$ given in eqs. (3) and (4).

The derivative of $g(\cdot)$ w.r.t. $\lambda$ at $\lambda=0$ is relevant for the DTTL loop bandwidth in the linear case and is given by

$$\left.\frac{dg(\cdot)}{d\lambda}\right|_{\lambda=0}=(2P_t)\cdot\left[erf\left(\sqrt{\frac{E_S}{N_o}}\right)-\frac{1}{2}(1-P_t)\exp\left(-\frac{E_S}{N_o}\right)\sqrt{\frac{E_S}{N_o}}\right] \tag{A.8}$$

which approaches

$$\left.\frac{dg(\cdot)}{d\lambda}\right|_{\lambda=0}\rightarrow(2P_t) \tag{A.9}$$

for high $(E_S/N_o)\gg 0$ dB.

*Appendix B*

We evaluate the mean value of $z=sgn(y)$ with $y=a+n$, i.e.,

$$\mathbf{E}[z]=\mathbf{E}[sgn(y)]=\mathbf{E}[sgn(a+n)]$$

where $a$ is a constant, and $n$ is a zero-mean Gaussian random variable of probability density function (pdf) $p_n(n)$ and variance $\sigma_n^2$. It follows

$$\mathbf{E}[z]=-\int_{-\infty}^{0}p_y(y)dy+\int_0^{\infty}p_y(y)dy$$

with $p_y(y)$ for the Gaussian pdf of $y$ with mean value $a$ and variance $\sigma_n^2$. Using

$$\int_{-\infty}^{0} p_y(y)dy = \frac{1}{2} \cdot \left[1 - erf\left(\frac{a}{\sigma_n\sqrt{2}}\right)\right]$$

we obtain

$$\mathbf{E}[sgn(a+n)] = erf\left(\frac{a}{\sigma_n\sqrt{2}}\right)$$

*Appendix C*

We evaluate the mean value of $z = n \cdot sgn(y)$ with $y = a + n$, i.e.,

$$\mathbf{E}[z] = \mathbf{E}[n \cdot sgn(y)] = \mathbf{E}[n \cdot sgn(a+n)]$$

where $a$ is a constant, and $n$ is a zero-mean Gaussian random variable of pdf $p_n(n)$ and variance $\sigma_n^2$. It follows

$$\mathbf{E}[z] = -\int_{-\infty}^{-a} n \cdot p_n(n)dn + \int_{-a}^{\infty} n \cdot p_n(n)dn$$

Simple integration leads to

$$\mathbf{E}[n \cdot sgn(a+n)] = \sqrt{\frac{2}{\pi}}\sigma_n \exp\left(-\frac{a^2}{2\sigma_n^2}\right) \quad \text{(C.1)}$$

Next, we evaluate the mean value of $z = n_1 \cdot sgn(y)$ with $y = a + n_1 + n_2$, i.e.,

$$\mathbf{E}[z] = \mathbf{E}[n_1 \cdot sgn(y)] = \mathbf{E}[n_1 \cdot sgn(a+n_1+n_2)]$$

where $a$ is a constant, and $n_1$ and $n_2$ are zero-mean, statistically independent Gaussian random variables with variances $\sigma_{n_1}^2 = \sigma_{n_2}^2 = \sigma_n^2$. It follows

$$\mathbf{E}[z] = \int_{-\infty}^{\infty}\left[\int_{-\infty}^{\infty} n_1 sgn[(a+n_2)+n_1]p_{n_1}(n_1)dn_1\right] \cdot p_{n_2}(n_2)dn_2$$

For the inner integration we consider $(a+n_2)$ as a constant, and we apply the result stated in eq. (C.1). Simple integration leads as follows:

$$\mathbf{E}[z] = \frac{\sigma_n}{\sqrt{\pi}} \exp\left(-\frac{3a^2}{4\sigma_n^2}\right)$$

## REFERENCES


[1] "Huygens Recovery Task Force (HRTF), Final Report," *European Space Agency*, Ref. HUY-RP-12241, Issue 1, 27 July 2001.

[2] L. Popken, "PSA Receiver Symbol-Synchronizer Dynamical Model," Technical Note, *European Space Agency*, Issue 2, 5 May 2003; and corresponding Author's Notes.

[3] L. Popken, "Probe Relay RF Link Modeling," Technical Note, *European Space Agency*, Issue 1, 2 April 2003.

[4] K. Andrews, "$E_S/N_o$ from Experimental Data," JPL E-Mail Correspondence, 10 April 2001.

[5] "Cassini-Huygens Integrated Data Link Report," Ref. ESA-JPL-HUY-25999, Issue 2, November 2003.

[6] L.J. Deutsch, "Resolving the Cassini/Huygens Relay Radio Anomaly," IEEE Aerospace Conference Proceedings, Big Sky, Montana, March 2002, Vol. 3, pp. 3-1295 – 3-1302.

[7] W.C. Lindsey, M.K. Simon, *Telecommunication Systems Engineering*, New York: Dover Publications Inc., 1991.

[8] Consultative Committee for Space Data Systems, *TM Synchronization and Channel Coding*, CCSDS 131.0-B-1, Blue Book, September, 2003.

[9] A. Papoulis, *Probability, Random Variables, and Stochastic Processes*, Second Edition, New York: McGraw-Hill, 1986.

[10] R.J. Baker, *CMOS, Mixed-Signal Circuit Design*, IEEE Press, 2002.


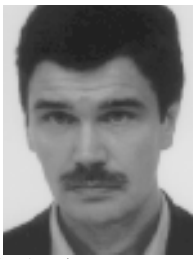


***Luitjens Popken*** *received his Dipl.-Ing. degree in Telecommunications. He serves as Principal Electrical Systems Engineer in the Scientific Programme Directorate of the European Space Agency. He was the Electrical Systems Engineer for the ESA satellite INTEGRAL (International Gamma-Ray Astrophysics Laboratory) during its development, which was concluded by the launch in October 2002 and by a very successful commissioning. He is now a member of the Science Projects Systems Office providing technical support to various Scientific projects on their on-going development and operational phases. In addition to his heavy involvement in the INTEGRAL Project, he was in 2000 assigned to the Huygens Recovery Task Force and subsequent Implementation Team.*

*Luitjens Popken has authored and co-authored around thirty conferences papers and journal publications. He is a Senior Member of the IEEE.*